Mah, R. S. H., "Structural Decomposition in Chemical Engineering Computation," 72nd AIChE Nat. Meeting, St. Louis (May 21-26, 1972).
Mah, R. S. H., and M. Shacham, "Pipeline Network Design and Synthesis," *Adv. Chem. Eng.*, **10**, 125 (1978).
Sargent, R. W. H., "The Decomposition of Systems of Procedures and Algebraic Equations," G. A. Watson, Ed., *Numerical Analysis-Proceedings*, Biennial Conf., Dundee, Lecture Notes in Mathematics 630, 158, Springer-Verlag, Berlin (1978).
Shacham, M., S. Macchietto, L. F. Stutzman, and P. Babcock, "Equation Oriented Process Flowsheeting," *Comp. Chem. Eng.*, **6**(2), 79 (1982).
Soylemez, S., and W. D. Seider, "A New Technique for Precedence-Ordering Chemical Process Equation Sets," *AIChE J.*, **19**, 934 (1973).

Manuscript received April 2, 1982; revision received December 6, and accepted December 14, 1982.

Fate of Solids Fed Pneumatically through a Jet into a Fluidized Bed

IFIYENIA KECECIOGLU, WEN-CHING YANG, and D. L. KEAIRNS

Westinghouse Research and Development Center
Pittsburgh, PA 15235

Solid tracer particles were fed pneumatically through a jet into a fluidized bed to simulate the feeding of solids via a pneumatic transport line into a fluidized-bed reactor operating in the slugging-bed mode. The fluidized bed was defluidized instantaneously at different times after the initiation of the tracer particle injection. The bed was then sampled layer by layer to provide the radial and axial concentration profiles of the tracer. Regular and high-speed movies (1,000 frames per second) were taken to study the operation of the fluidized bed and the phenomena of the gas-solid two-phase jet.

Experimental results on solid mixing, jet constriction and slugging frequencies, slugging bed height, slug length, jet penetration, and jet half-angle at three nominal jet velocities of 52, 37, and 25 m/s and corresponding solids loadings are presented. Additional experimental results on jet constriction and slugging frequencies, and slug volume (axial slug size) obtained for a wider range of jet velocities confirm the hydrodynamic trends observed during the tracer particle injection experiments. The results indicate that solids mixing increases, and well-mixed conditions are reached earlier, with an increase in jet injection velocity. The obtained mixing times were correlated successfully in terms of the excess gas velocity. The experimental data on jet penetration and slug motion were satisfactorily correlated by modified versions of existing theoretical relations. The modifications included the effect of the injected solids on jet penetration and jet half-angle and also the effect of our semicircular column geometry and single wall-slug configuration on the observed slug motion.

SCOPE

Fluidized-bed reactors have been widely acclaimed in the process industry for their advantageous characteristics of good mixing, high rates of heat and mass transfer, mechanical robustness, and capability of continuous operation. Research seeking to harness these favorable reactor characteristics to the efficient and environmentally acceptable processing of fossil fuels (e.g., coal combustion, coal and oil shale gasification) has been undertaken intensively in recent years.

In gas-solid fluidized beds, the gaseous reactant is introduced uniformly through a distributor plate, while the solids are introduced via individual feed points. As a result, one has to rely on the characteristics of the flow field to promote solids mixing within the reactor.

A commonly employed method of feeding solids into a fluidized bed is pneumatic injection of the solids through a two-phase gas-solid jet. If the gas-solid reaction is fast, undesirable, localized, nonuniform temperature and concentration conditions may appear around the solids feeding points in the fluidized bed. Such an occurrence may compromise the performance of the fluidized-bed reactor. Therefore, from the points of view of reactor design and selection of optimum reactor operating conditions, knowledge of the particle history inside the fluidized bed is essential.

The fate of solids fed pneumatically through a jet into a fluidized bed depends on the particle size and density, the jet velocity, the solid loading in the jet, the bed height, the bed diameter, the jet nozzle design, and the fluidization conditions in the bed. Despite the importance of the fate of pneumatically fed solids to reactor performance, the complex phenomena affecting solids mixing have not as yet been studied systematically.

A simple but effective technique was developed in this study to determine the extent of solids mixing and the deviation from the ideal flow patterns in different regions within a fluidized-bed reactor by sampling the injected solid tracer particles upon defluidization.

Experimental results on solids mixing and the related flow field phenomena in a slugging fluidized bed are presented at three nominal jet velocities of 52, 37, and 25 m/s. The experiments were performed at atmospheric pressure and ambient temperature.

CONCLUSIONS AND SIGNIFICANCE

The conclusions derived from the particle mixing experiments and their significance are summarized below:

(1) From the concentration profiles of the tracer particles, we have concluded that an increase in the jet injection velocity enhances the mixing of solids inside the fluidized bed. The solids attained the well-mixed condition within 50 seconds for the lowest jet injection velocity of 25 m/s, and within 30 seconds for the intermediate jet injection velocity of 37 m/s; for the highest jet injection velocity of 52 m/s, the corresponding time was reduced to approximately 20 seconds.

(2) The slugging mechanism and its associated bulk solids movement play an important role in the radial and axial dispersion of tracers, particularly in the slugging upper sections of the fluidized bed. The solids circulation induced by the jet improves the degree of mixing of the adjacent solids in the jetting lower portion of the bed within a conical zone of influence which is related to the frictional material properties of the bed solids and the degree of fluidization around the jet.

(3) The momentum of the injected solids can be an important fraction of the momentum of the injected dilute two-phase gas-solid stream because of the high injected solid particle velocity. The injected tracer particles tended to accumulate at the top of the jet. This suggests that the rate at which the solids are fed into the jet is much higher than the rate at which they are recirculated. It also suggests that the residence time of the injected solids in the jet region per pass is much longer than the time of their travel to the top of the jet.

(4) The observed average jet penetration length is satisfactorily predicted by the existing correlation of Yang and Keairns (1978) and Yang (1981) when it is appropriately modified to take into account the momentum of the injected solids (Eq. 2). Accordingly, the jet penetration is primarily dominated by the balance of the inertial forces of the gas jet and the injected solids and the gravitational force of the bed. Alternatively, the jet penetration length can also be predicted if the maxima in the tracer concentration profiles for short tracer injection durations are associated with the jet penetration length (Table 3). The observed average jet half-angle of $\theta \simeq 8.0°$ compares favorably with findings of other investigators (Rushton, 1980; Anagbo, 1980; Merry, 1975; Themelis et al., 1969; Donald and Singer, 1959). Comparison of the calculated values for jet half-angle (Eqs. 8 and 9) with our experimental results confirms our visual observations of the narrowing of the jet half-angle when the injection of the tracer particles is initiated. These observations are important for formulating a realistic gas-solid reaction model for the jet region.

(5) The experimental observations on maximum slugging bed height agree well with the predicted values given by the modified Matsen et al. (1969) correlation (Eq. 10, Table 5). The experimentally observed slugging frequencies (f_{SF}) are independent of the superficial gas velocities; however, the axial dimension of the slugs and the associated bulk solids movement increase with an increase in superficial gas flow. The slug lengths are satisfactorily predicted by Eq. 12 (Figure 14) in terms of the excess gas velocity, the solids spacing, and an empirical emulsion-phase velocity shape factor. The slugging frequencies are satisfactorily predicted by Eq. 14 (Figure 15). Accordingly, the slugging frequency probably depends on the frictional material properties of the bed solids. For our experiments, the data indicated that $f_{SF} \simeq 0.78$ Hz. These observations are important for improving our understanding of slugging and its effect on solids mixing.

(6) The nondimensional mixing times, $\tau/(1/f_{SF})$, were satisfactorily correlated as a function of the nondimensional excess gas velocity $(U - U_{mf})/U_b$ by Eq. 15 (Figure 16). This correlation implies that, for the flow conditions prevalent in our cold flow reactor model, slugging is the hydrodynamically limiting mechanism for solids mixing.

INTRODUCTION

The properties of solid particles, such as size, density, shape, porosity and structural integrity, vary during the continuous operation of gas-solid fluidized systems as a result of physical and chemical processes. If the particle and gas residence times in a fluidized-bed reactor are small and the temperature and concentration profiles are nonuniform, the effect of the solid particle motion on the performance of the reactor may become important. Moreover, high solids circulation rates may enhance the importance of the motion of solids in the performance of the reactor.

In fluidized-bed reactors, high solids circulation rates are desirable from the points of view of:

(1) Promoting heat and mass transfer, which inhibits the development of high temperature spots that, for example, promote deposit formation

(2) Improving gas-solid interactions that enhance reaction rates, especially during the initial stages of reaction

(3) Enhancing solids mixing between reaction zones which may be essential for the proper performance of the reactor

(4) Mechanically controlling the size of the solid particles inside the reactor if it is desirable to do so.

In a fluidized-bed reactor, jets and bubbles induce high solids mixing. The presence of a high-velocity gas jet induces solids circulation because of the entrainment of solids into the jet along the jet length. Solids mixing due to the motion of bubbles at a certain frequency is induced primarily by the solids-carrying capacity of the bubble wake and by the displacement of the surrounding solids.

As a result of modeling and design needs, one must determine the extent of solids mixing and the deviation from the ideal flow patterns in different regions within a fluidized-bed reactor whenever nonuniform temperatures and gas-concentration profiles and higher circulation rates are encountered. The study of the fate of solids injected into a fluidized bed by means of a gas-solid two-phase jet would be of particular interest. Such a study would simulate the feeding of solids via a pneumatic transport line into an operating fluidized-bed reactor. The incoming jet stream of such a two-phase jet carries solid particles at different loadings. The momentum of these solid particles is not negligible, and, as shown later in this paper, it significantly affects the jet penetration length.

To study the fate of injected solids, solid tracer particles were fed pneumatically at a constant rate through a jet into a steadily pulsating fluidized bed (slugging and jet pulsation). The experiments were performed at ambient temperature and atmospheric pressure. Regular and high-speed movies (1,000 frames per second) were also taken to study the operation of the fluidized bed and the phenomena associated with the gas-solid two-phase jet.

In this paper we present experimental results on solids mixing, jet constriction and slugging frequencies, slugging bed height, slug volume (axial slug size), jet penetration, and jet half-angle at three nominal jet velocities (52, 37, and 25 m/s) in a 28.6 cm semicircular transparent (Plexiglas) fluidized-bed column. The corresponding solid loadings in the jet (weight of solids/weight of gas) were 1.8, 2.6 and 3.8, respectively. Additional experimental results on jet constriction and slugging frequencies, and slug volume (slug length) obtained for a wider range of nominal jet velocities provided further insight into the effect of the fluidized-bed hydrodynamics on solids mixing.

TABLE 1. PHYSICAL CHARACTERISTICS OF ACRYLIC BED MATERIAL AND POLYCARBONATE RESIN TRACER MATERIAL[a]

Acrylic Bed Material		Polycarbonate Resin Tracer Material	
Sieve Size (mesh)	wt. %	Sieve Size (mesh)	wt. %
14	0.0	5	0.0
20	39.6	6	1.0
30	45.3	8	95.9
40	13.0	10	3.1
50	2.1	PAN	0.0
PAN	0.0		
Average Particle Size (μm[b]): 770		Average Particle Size (μm[b]): 2,850	
Particle Density (kg/m^3): 1,190		Particle Density (kg/m^3): 1,200	
U_{mf} (cm/s): 25.5 (experimental)		U_{mf} (cm/s): 80.0 (experimental)	
U_t (cm/s): 370 (calculated)		U_t (cm/s): 930 (calculated)	
U_{cf} (cm/s): 33.5 (experimental)		U_{cf} (cm/s): 89.3 (experimental)	
ϵ_{mf}: 0.54 (experimental)		ϵ_{mf}: 0.4 (experimental)	
Angle of Repose[c]: 39° (experimental)			
Angle of Internal Friction[c]: 78 ° (experimental)			

[a] Fluid properties calculated at 20°C and 101.3 kPa.
[b] Calculated from $\bar{d}_p = 1/[\Sigma_i(x/d_p)_i]$
[c] Defined by Zenz and Othmer (1960).

EXPERIMENTAL APPARATUS AND PROCEDURE

Three series of experiments were performed to investigate the rate of particle mixing as a function of the jet injection velocity. The experiments were conducted in a semicircular transparent Plexiglas column, 28.6 cm in diameter (Yang and Keairns, 1978), Figure 1. The two-phase jet was introduced through a semicircular jet nozzle, 2.54 cm in diameter, with its flat side placed against the flat front plate of the apparatus. During the three series of particle mixing experiments, the top of the jet injection tube was kept at the level of the most narrow flow area of the 60-degree conical grid. The bed material was white acrylic with a mean particle diameter of 770 μm and density of 1.19 g/cm^3. The minimum fluidization velocity of the bed material was determined experimentally, in a separate 7.0 cm diameter bed, to be 25.5 cm/s. The physical characteristics of the bed material are summarized in Table 1. For the given mean particle diameter and density our bed material is classified as a group B powder (Geldart, 1973). As confirmed also by our experimental observations, group B powders bubble at or only slightly above minimum fluidization velocity. At minimum fluidization conditions the bed expansion is small and the bed collapses very rapidly when the gas supply is cut off. To provide a rough classification of the flowability of our powder, the angle of repose (angle formed when the powder is poured into a conical heap) was measured experimentally. With an angle of repose of 39°, our bed material is classified as a free-flowing powder (Hogg and Augenstein, 1978). The pneumatically introduced tracer solid particles had a mean particle diameter of 2850 μm and a density of 1.20 g/cm^3. The minimum fluidization velocity of the tracers was experimentally determined to be 80.0 cm/s. Accordingly, the tracer material, although coarser, has the same density as the main bed material and is therefore expected not to segregate and to follow the solids motion of the main bed material (Rowe et al., 1972).

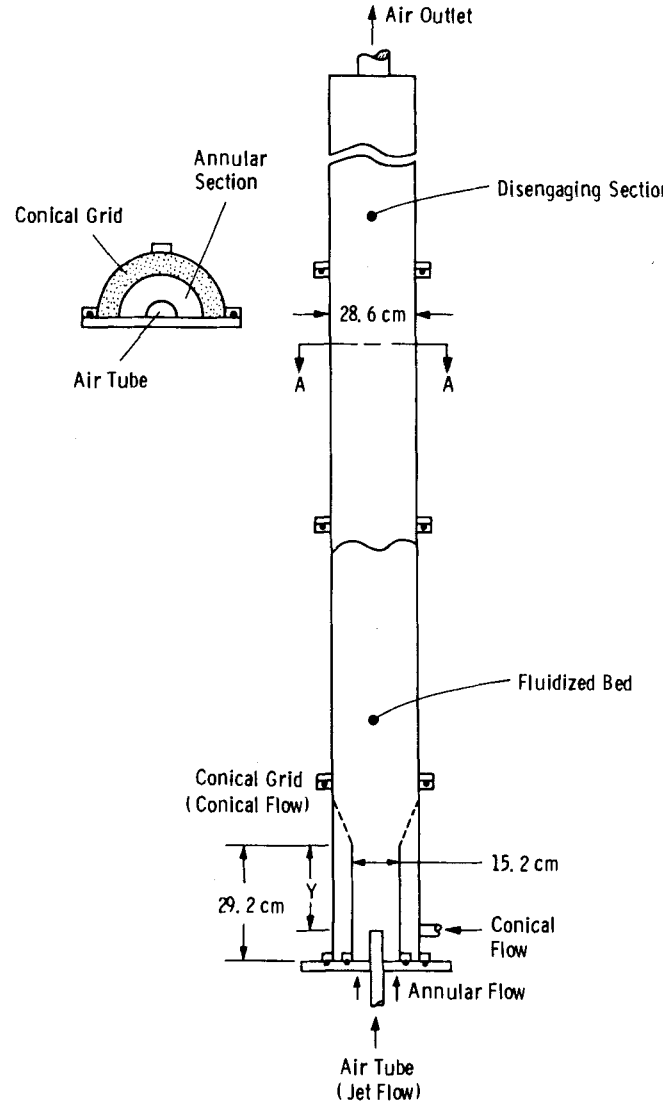

Figure 1. A schematic diagram of the test apparatus.

The tracer injection experiments were conducted at three different nominal jet velocities (25, 37 and 52 m/s) with corresponding solid loadings (weight of solids/weight of gas) of 3.8, 2.6 and 1.8, respectively. The static bed height was maintained constant at 103.0 cm from the top of the jet nozzle. The grid and annular flows were kept constant near the minimum fluidization flow rates for the acrylic bed material. The experimental conditions for the three series of experiments are summarized in Table 2. For these flow conditions the jet was in the pulsating bubbling mode and the fluidized bed was in the slugging mode. The solid tracer particles in the jet were delivered via a hopper and a variable-speed screw feeder into a 2.5 cm pneumatic transport line which was connected to the 2.5 cm semicircular jet nozzle. (The solids delivery rate had been calibrated beforehand at different gas flow rates; it was determined to be constant and equal to about 29 g/s.) The tracers were introduced into a steadily pulsating fluidized bed (slugging and jet pulsation). At 3, 5, 7, 10, 15, 20, and 30

TABLE 2. FLOW[a] CONDITIONS FOR PARTICLE MIXING EXPERIMENTS

Series No.	Jet Flow	Jet Velocity	U/U_{mf}	$\frac{U-U_{mf}}{U_b}$	$Re_j = \frac{U_j d_o \rho_f}{\mu_f}$	U_{sj}	$Re_j^* = \frac{U_m d_o}{\nu}$
1[b]	6.47×10^{-3} m^3/s	25.53 m/s	1.84	0.32	43,862	8.40 m/s	142,643
2[b]	9.46×10^{-3} m^3/s	37.34 m/s	2.21	0.46	64,153	10.00 m/s	167,416
3[b]	13.21×10^{-3} m^3/s	52.15 m/s	2.67	0.64	89,597	14.35 m/s	185,367

[a] The flows were calculated at 20°C and 101.3 kPa.
[b] Annular flow = 3.04×10^{-3} m^3/s; grid flow = 5.54×10^{-3} m^3/s.

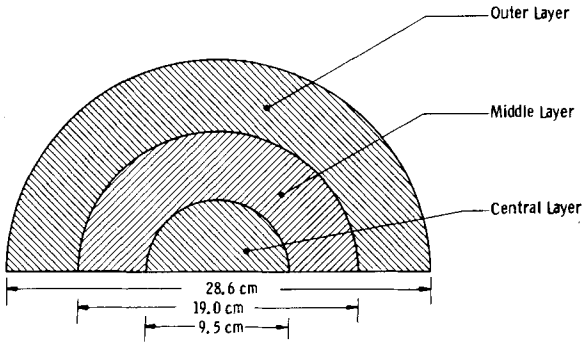

Figure 2. Dimensions of the three radial sampling layers.

seconds after the initiation of the tracer particle injection, the fluidized bed was defluidized instantaneously. (Additional tracer injection experiments were performed to provide a more complete picture of solids mixing. They included one tracer injection experiment for 50 s for the first series and another for 40 s for the second series.) The bed was then sampled layer by layer to provide the radial and axial concentration profiles of the tracer. The sampling procedure of the defluidized bed was such that at each axial location, three 5.08 cm thick samples were obtained at three different radial locations. Figure 2 shows the dimensions of the three radial sample volumes. Each sample was removed from the defluidized bed by vacuuming. For each sampled layer the tracer particles were separated from the main bed material through sieve analysis, and the weights of the main bed material and the tracers of each sampled layer were recorded. In each experimental run the sampling started at the top of the defluidized bed and proceeded downward toward the conical grid. The detailed sampling was terminated at the top of the conical grid plate.

Regular and high-speed movies (1,000 frames per second) were also taken to study the operation of the fluidized bed and the phenomena of the gas-solid two-phase jet. The camera was mounted normal to the flat face of the semicircular Plexiglas fluidized-bed apparatus. The movies were then analyzed frame by frame using a motion analyzer to record the tracer particle trajectories and the tracer particle velocities during their injection into the steadily fluidized bed. From the analysis of the movies, we obtained information about jet constriction and slugging frequencies, slugging bed height, slug volume (axial slug size), jet half-angle and jet penetration length, for the three nominal jet velocities of 25, 37, and 52 m/s.

For the purpose of obtaining a more thorough understanding of the trends observed during the tracer particle injection experiments, an auxiliary set of experiments was performed to provide information on the gross behavior of the cold flow model as a function of the jet injection velocity and the flows through the conical grid and the annulus.

EXPERIMENTAL RESULTS

The following results were obtained from the three series of tracer particle injection experiments and the auxiliary set of experiments.

Tracer Particle Mixing

The data obtained from the tracer particle mixing experiments were plotted as a function of axial distance for each radial location. The deviation of the data from the uniformly mixed condition was evaluated by plotting the ratio of the weight fraction of tracer particles in the sampled volume to the weight fraction of tracer particles in the entire bed (i.e., $\overline{C}_T$) as the ordinate and axial location for each radial layer as the abscissa. For a uniformly mixed condition in a given layer, this ratio should be equal to unity. Moreover, to obtain an objective indicator of the deviation of the tracer concentration profiles from the ideal or uniformly mixed state, a root-mean-square concentration deviation from the well-mixed condition was defined as:

$$d_{RMS} \equiv \left(\frac{1}{V}\int_0^V (\overline{C}_T - 1)^2 dV\right)^{1/2}, \qquad (1)$$

where V is the volume of the sampled bed solids.

A nearly-well-mixed criterion of $d_{RMS} \simeq 0.5$ was chosen to imply that the mixing of solids is relatively complete from the point of view of design considerations. A $d_{RMS} \to 0.5$ appears also to be an indicator of a long-term mixing state, especially for the outer sampling layer, because of the presence of dead zones of solid

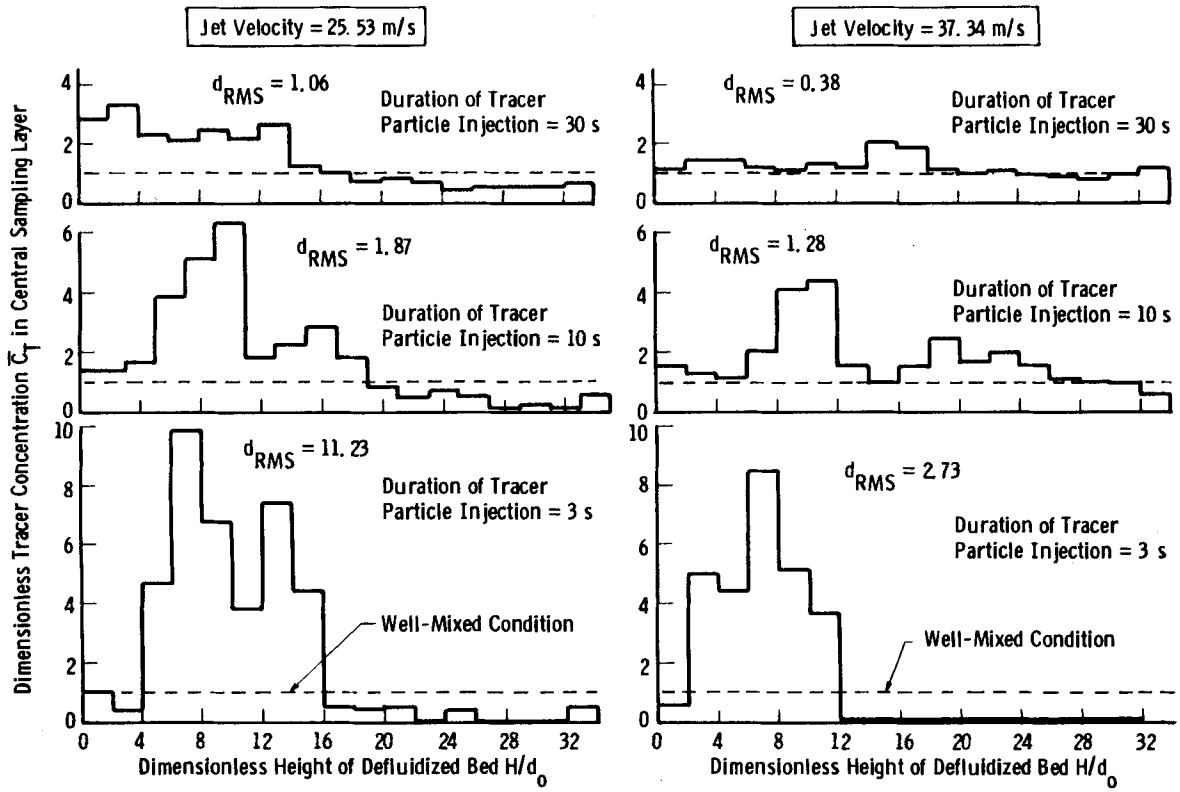

Figure 3. Solid mixing in central sampling layers during tracer particle injection for jet injection velocities of 25 m/s and 37 m/s (grid flow = 5.54 × 10^{-3} m^3/s; annular flow = 3.04 × 10^{-3} m^3/s).

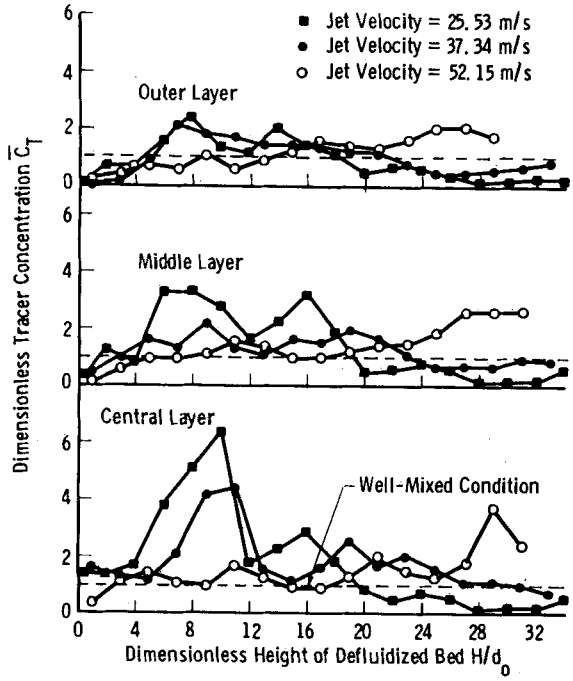

Figure 4. Tracer mixedness as a function of jet injection velocity for tracer particle injection duration of 10 seconds (grid flow = 5.54 × 10^{-3} m³/s; annular flow = 3.04 × 10^{-3} m³/s).

mixing in the flow field in the jetting portion of the fluidized bed, as mentioned later.

The axial and radial tracer concentration profiles obtained from the tracer particle injection experiments show that:

- For the two lower jet injection velocities (25 and 37 m/s) and for short tracer injection durations, up to 10 seconds, the tracer concentration profiles inside the bed show that the solids are not well mixed but are concentrated primarily in the lower portion of the bed around the jet.
- For the jet injection velocities of 25 and 37 m/s, the variation in the tracer concentration profiles beyond 10 seconds is gradual. Within 30 seconds the solids are nearly well mixed in the series of

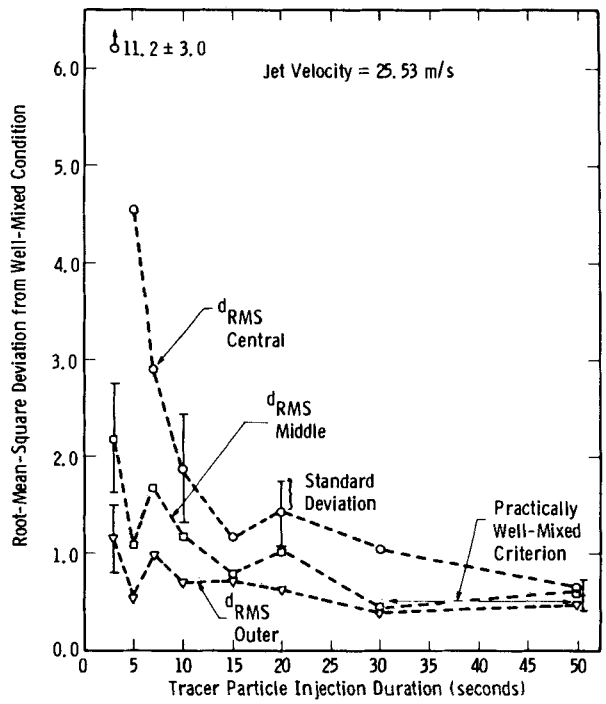

Figure 5. Root-mean-square deviation from well-mixed condition as a function of tracer particle injection duration for a jet injection velocity of 25 m/s.

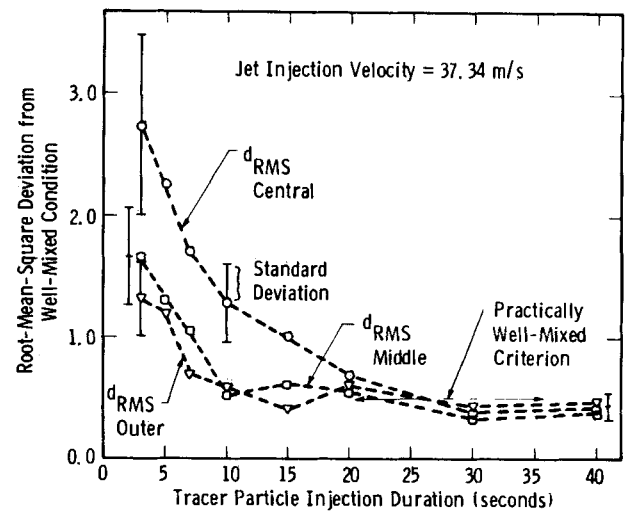

Figure 6. Root-mean-square deviation from well-mixed condition as a function of tracer particle injection duration for a jet injection velocity of 37 m/s.

experiments with the higher jet injection velocity of 37 m/s (Figures 3, 5 and 6). For the jet injection velocity of 25 m/s, the tracer particles attained the nearly well-mixed conditions within 50 seconds (Figures 5 and 9).

- For the highest jet injection velocity of 52 m/s, the tracer particles reach the top of the bed much faster and the well-mixed condition is attained much sooner. Within 20 seconds the solids are nearly well mixed (Figures 4 and 7).
- From the concentration profiles of tracer particles in the three different series of experiments, we can deduce that the increased jet injection velocity enhances the mixing of solids inside the fluidized bed (Figures 5 through 7).
- From the concentration of the tracers in the outer sampling layer, for short tracer injection durations the slugging mechanism appears to be a major driving force in the radial and axial dispersion of tracers, particularly at the upper slugging sections of the fluidized bed (Figure 8). The solids circulation induced by the jet affects the degree of mixing of the adjacent solids mainly in the lower jetting portion of the bed. From the tracer concentration data of Figures 8 and 9 one can see that in the lower portions of the outer sampling layer, near the conical distributor plate, the solids mixing

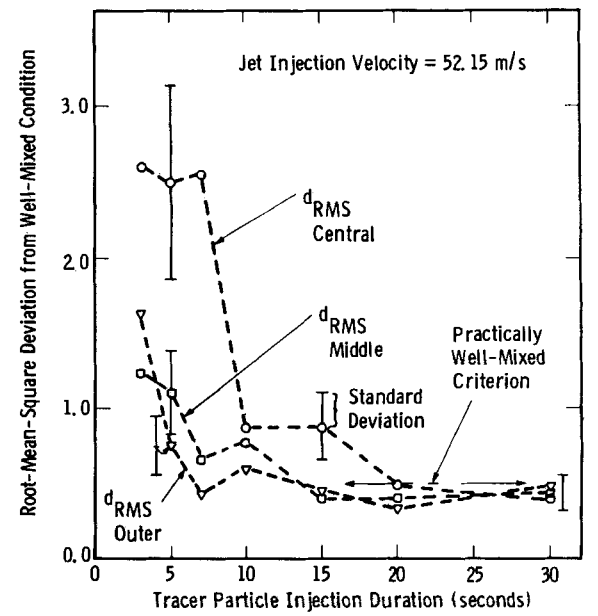

Figure 7. Root-mean-square deviation from well-mixed condition as a function of tracer particle injection duration for a jet injection velocity of 52 m/s.

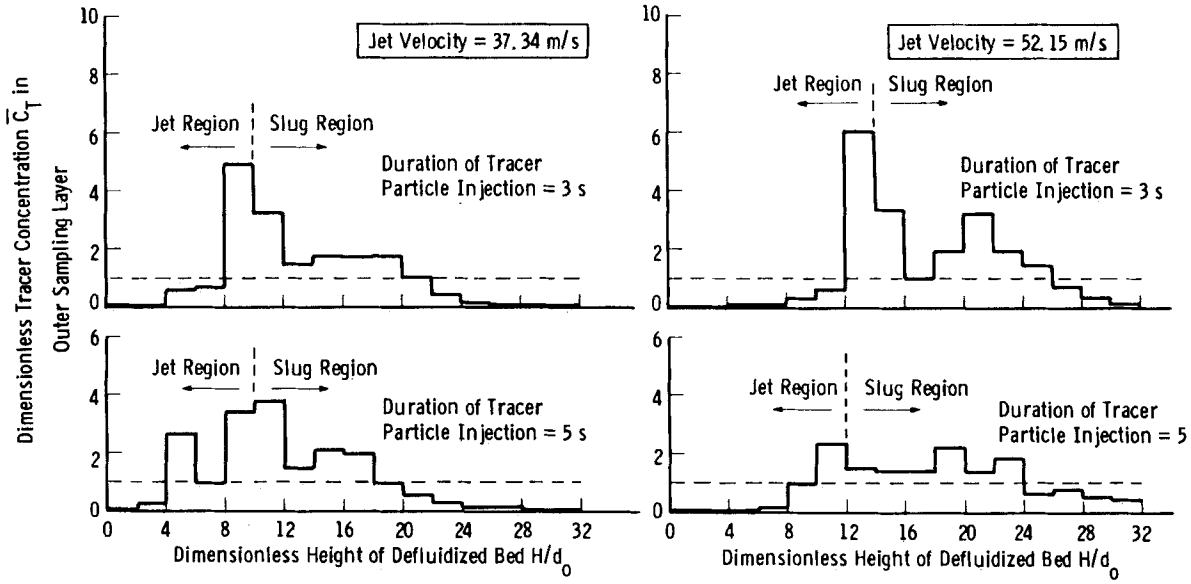

Figure 8. Effect of slugging on axial and radial dispersion of injected tracers in upper sections of fluidized bed for jet injection velocities of 37 m/s and 52 m/s (grid flow = 5.54 × 10^{-3} m^3/s; annular flow = 3.04 × 10^{-3} m^3/s).

is not adequate. This supports our visual observations that the jet affects the solids flow conditions inside a conical zone of influence which is centered at the jet injection tube (Figure 10).

The angle of the cone of influence of the jet α is a weak function of the jet injection velocity. From the tracer particle concentration profiles in the lower portions of the outer sampling layer α is calculated to be about 73°. (The distance L (Figure 10) was obtained by relating the corresponding defluidized-bed height to the fluidized-bed state using Eq. 3. The derivation of this equation is explained in the section on jet penetration length based on the dissipation of solids momentum inside the jet.) This value of α agrees well with our visual observations and is close to the value of the angle of internal friction of the granular solid bed material, which was independently determined to be about 78° according to the procedure outlined by Zenz (1960).

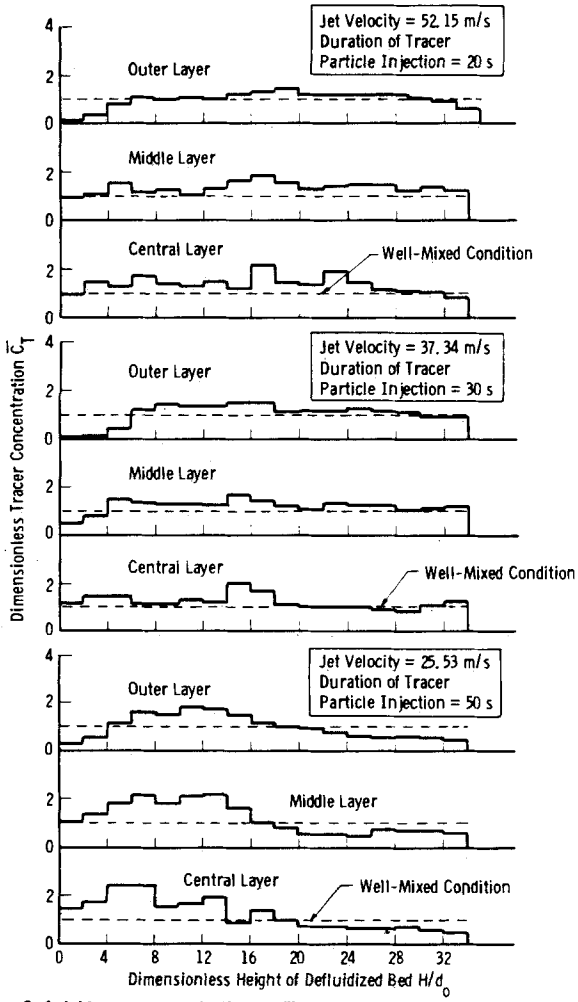

Figure 9. Axial tracer concentration profiles for practically well-mixed condition for all radial sampling layers and for injection velocities of 25 m/s, 37 m/s, and 52 m/s (grid flow = 5.54 × 10^{-3} m^3/s; annular flow = 3.04 × 10^{-3} m^3/s).

Jet Penetration Length

With the aid of regular and high-speed movies, we obtained experimental information on the jet penetration length, the trajectories, and the velocities of the injected tracer particles.

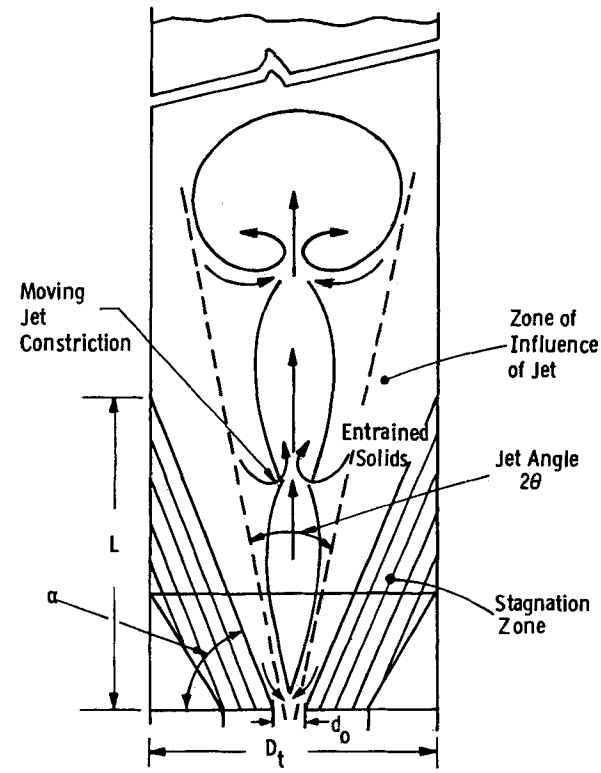

Figure 10. Zone of influence and stagnation zones around jet; solid circulation pattern induced by central jet.

For our flow conditions the jet was in a pulsating bubbling mode. The fluctuation in the jet penetration length due to this pulsation made it difficult to determine a well-defined single value for the jet penetration length at a particular jet velocity. In this investigation, therefore, the reported jet penetration, which was obtained from visual observations of videotape recordings and movies at 64 frames per second, is the time-average value of the observed jet penetration lengths.

A typical jet consisted of a dilute gas-solid two-phase mixture followed by a series of bubbles that originated at the top of the jet. The dilute phase contained the injected tracer particles and solids entrained into the jet along its length. At minimum jet penetration length (L_{min}) the jet had the shape of a flame; at maximum jet penetration length (L_{max}) it had the appearance of a series of coalescing bubbles with periodic regions of constriction. Figure 11 shows the jet configurations for maximum and minimum jet penetration during the second series of experiments; it also shows the way L_{min} and L_{max} were measured.

The measured average jet penetration length is satisfactorily predicted when the existing correlation of Yang and Keairns (1978) and Yang (1981) is modified to take into account the momentum of the injected solids. This modification assumes that the jet penetration is primarily dominated by the balance of the inertial forces of the gas jet and the injected solids and the gravitational force of the bed. Then,

$$\frac{L_j}{d_o} = 6.5\left(\frac{M_f U_f + M_{sj}U_{sj}}{(\rho_s - \rho_f)g d_o}\right)^{1/2} = 6.5\left(\frac{\epsilon\rho_f U_f^2 + (1-\epsilon)\rho_{sj}U_{sj}^2}{(\rho_s - \rho_f)g d_o}\right)^{1/2}. \quad (2)$$

All of the quantities listed above [with the exception of ϵ were determined experimentally. The quantity ϵ was derived from the definition of the injected solids mass flux, $M_{sj} \equiv (1-\epsilon)\rho_{sj}U_{sj}$. The agreement between the theoretical values for jet penetration length and the experimentally observed values is very good. A comparison of these values is provided in Table 3. This table also shows the percentage increase in the theoretical jet penetration length due to the inclusion of the injected solids momentum. This appreciable increase in the predicted jet penetration length suggests that the momentum of the injected solids can be an important factor in the delineation of the jet boundaries.

When rigorously written, the term in the denominator of Eq. 2, which represents the gravitational force of the bed, should be multiplied by the solid volume fraction around the jet region. The bed around the jet region is expected to be essentially at minimum fluidization condition; therefore, for a given bed material the solid volume fraction is assumed to be constant. In the correlation of Eq. 2 the effects of the surrounding solid volume fraction and other secondary phenomena governing the behavior of the two-phase jet are lumped in the constant multiplying the Froude number.

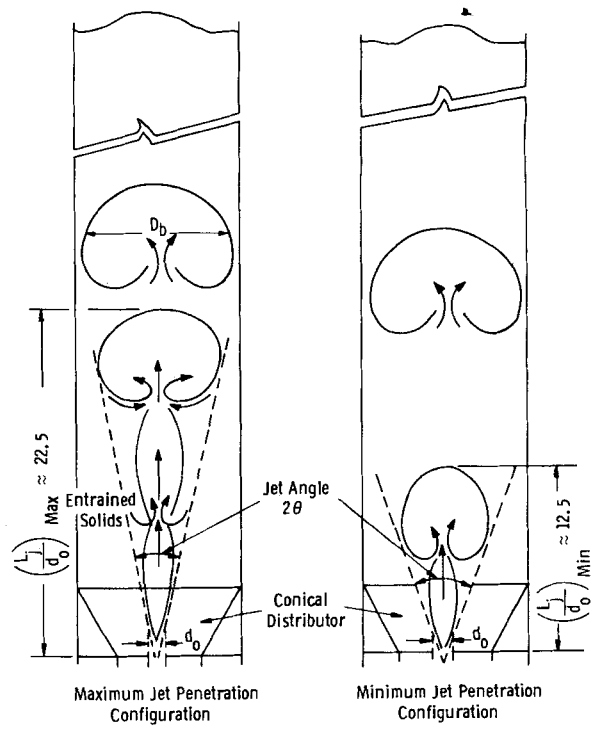

Figure 11. Observed jet penetration configurations and definitions of jet penetration length.

As stated earlier, a major uncertainty and ambiguity in studying jets in fluidized beds lies in the definition of jet penetration length. According to Merry (1975), the jet penetration length is the height at which the jet degenerates into a gas bubble, and the truncation of the jet occurs always at the jet nozzle. In our case, however, a jet was always present inside the fluidized bed. The jet configuration changed from that at L_{min} to that at L_{max} (Figure 11), at which point the bubble that formed above L_{max} detached and the jet went back to its minimum configuration. Accordingly, the definition of the jet penetration length was modified to take into account these phenomena.

Another definition of jet penetration length may be based on the dissipation of solids momentum inside the jet. Then the maxima in the tracer concentration data (L_{MC}) for short tracer injection durations can be related to the jet penetration length. The above hypothesis is based on the assumption that the tracers are likely to

TABLE 3. JET PENETRATION LENGTH: EXPERIMENTAL VALUES AND COMPARISON WITH PREDICTIONS OF CORRELATIONS

Series No.	1	2	3
Experimental L_j/d_o (Visual Observation[a])	15.6 ± 3.0	19.8 ± 4.0	25.4 ± 5.6
Experimental L_j/d_o, Eq. 3 (From Max. Concentration)	15 ± 3	19 ± 3	25 ± 3
Corresponding Jet Vol.: $V_j = A \times (H_{min} - H_{mf})$	2440 cm^3 (20%)[b]	3260 cm^3 (21%)[b]	5700 cm^3 (29%)[b]
L_j/d_o, Eq. 2 (% Increase in L_j/d_o Due to Injected Solids Momentum)	15.8 (50%)	20.0 (30%)	26.3 (22%)
L_j/d_o, Eq. 4: (U_f, ρ_f)	9.9	11.8	13.8
L_j/d_o, Eq. 4: (U_f, ρ_m)	21.1	24.0	25.2
L_j/d_o, Eq. 4: (U_m, ρ_m)	10.8	12.2	13.8
L_j/d_o, Eq. 5: (U_f, ρ_f)	5.9	7.3	8.7
L_j/d_o, Eq. 5: (U_m, ρ_m)	15.9	16.4	16.1
L_j/d_o, Eq. 6: (U_f, ρ_f)	19.8	27.7	37.3
L_j/d_o, Eq. 6: (U_m, ρ_m)	34.6	41.1	48.1

[a] Time-average value ± standard deviation.
[b] Percentage calculated as $[V_j/(A \times L_j)] \times 100$.

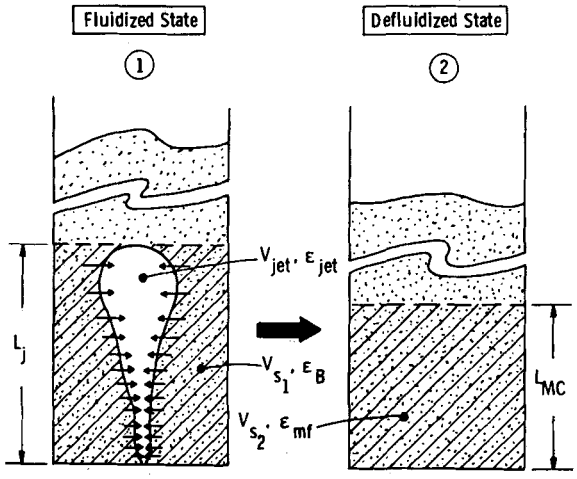

$$V_{s_1} = (1-\varepsilon_B)[A L_j - V_{jet}\varepsilon_{jet}]$$

$$V_{s_2} = (1-\varepsilon_{mf}) A L_{MC}$$

$$V_{jet} = A(H_{min} - H_{mf})$$

$$\varepsilon_B \simeq \varepsilon_{mf};\ \varepsilon_{jet} \cong 1;\ V_{s_1} = V_{s_2}$$

$$\Rightarrow \boxed{L_j = L_{MC} + (H_{min} - H_{mf})}$$

Figure 12. Defluidization process around jet.

gather near the top of the jet where they hit the barrier of relatively motionless and more densely packed solids in the fluidized bed. Moreover, we have assumed that during defluidization, which is complete within approximately 0.3 seconds, the gap that was occupied by the jet is filled primarily with bed material from the radially adjacent layers. These solids move radially inward as the bubble that remains in place of the jet (after the air flow has been turned off) moves upward and disappears. The model for the defluidization process around the jet is depicted in Figure 12.

During the operation of the slugging fluidized bed, the bed height oscillated between a minimum and a maximum value as the slug that originated at the top of the jet moved through the bed and disappeared. The minimum bed height was consistently above the height of the bed at minimum fluidization conditions when no central jet was present. The difference between the minimum bed height (H_{min}) and the bed height at minimum fluidization conditions (H_{mf}) is taken to be due to the volume occupied by the jet (V_j). Then, $V_j = A \times (H_{min} - H_{mf})$. Table 3 shows values of the calculated jet volumes for the three series of experiments. As a result, as shown in Figure 12,

$$L_j = L_{MC} + (H_{min} - H_{mf}). \tag{3}$$

The jet penetration length values obtained from the above equation agree well with the experimental observations from movies and videotape recordings, as well as with the values obtained from the correlation of Eq. 2 (Table 3).

Comparison of our data with predictions of other correlations available in the literature is also included in Table 3. The correlations selected for comparison are the ones quoted most frequently in the literature and are those by Merry (1975), by Hirsan et al. (1980), and by Wen et al. (1982). These correlations were selected because they are expressed in terms of nondimensional groups of physical variables and because their derivations are based either on dimensional analysis or on semitheoretical arguments.

Merry (1975) assumed that the volume of the bubble that was generated at the end of the jet could be calculated by the equation derived by Davidson and Harrison (1963; pp 50–62). By empirically correlating the jet half-angles reported in the literature, he arrived at the following equation for jet penetration:

$$\frac{L_j}{d_o} = 5.2\left(\frac{\rho_f d_o}{\rho_s d_p}\right)^{0.3}\left[1.3\left(\frac{U_f^2}{g d_o}\right)^{0.2} - 1\right]. \tag{4}$$

Hirsan et al. (1980) analyzed their own high pressure jet penetration data and suggested the following correlation:

$$\frac{L_j}{d_o} = 19.3\left(\frac{\rho_f U_f}{\rho_s \sqrt{g d_p}}\right)^{0.83}\left(\frac{U}{U_{cf}}\right)^{-0.54}. \tag{5}$$

The equation for jet penetration length by Wen et al. (1982) was obtained from dimensional analysis by correlating the atmospheric pressure data by Yang and Keairns (1978) and the elevated pressure data (up to 53 atm) of Knowlton and Hirsan (1980). Their proposed correlation is:

$$\frac{L_j}{d_o} = 1.3\left(\frac{U_f^2}{g d_p}\right)^{0.38}\left(\frac{\rho_f d_p U_f}{\mu}\right)^{0.13}\left(\frac{\rho_f}{\rho_s}\right)^{0.56}\left(\frac{d_o}{d_p}\right)^{0.25}. \tag{6}$$

During our experiments, the fluid injected through the jet was a gas-solid two-phase mixture. When rigorously written, therefore, the jet nozzle velocity U_f and the injected fluid density ρ_f in the above equations should in most cases be replaced by the average mixture velocity U_m and the mixture density ρ_m, respectively, where

$$\rho_m = \epsilon\rho_f + (1-\epsilon)\rho_{sj} \tag{7a}$$

and

$$\rho_m U_m^2 = \frac{M_f U_f + M_{sj} U_{sj}}{(\pi d_0^2/8)}. \tag{7b}$$

In Table 3, two predicted values of jet penetration length are listed for the last two of the above correlations. They include one calculation in which the terms in the correlations have not been modified and another calculation in which the injected fluid density ρ_f and injected fluid velocity U_f hve been replaced by their corresponding fluid mixture values ρ_m and U_m. There are three predicted jet penetration lengths listed for Merry's correlation (1975). These values correspond to the jet penetration length predicted by the unmodified correlation, a calculation in which the values for ρ_f and U_f in the correlation have both been replaced by ρ_m and U_m, and a calculation in which only ρ_f has been replaced by ρ_m. This last case suggests that only the predicted jet half-angle is affected by the presence of the solids in the injected gas-solids mixture while the volume of the gas bubble at the end of the jet depends primarily on the injected gas flow rate and its shape is unaffected by the presence of solids in the injected stream.

In conclusion, the tabulated results of the comparison of our data with predictions of jet penetration correlations suggest that the jet penetration length values calculated from the correlation of Eq. 2 are more accurate and that they are also more sensitive to the changes in the experimental conditions than the values predicted by the other quoted correlations.

Jet Half-Angle

In our fluidized-bed cold-flow model we observed a pulsating bubbling jet, the maximum and minimum configurations of which, for the intermediate jet injection velocity, are depicted in Figure 11. Accordingly, the jet is assumed to be symmetrically located with respect to the jet nozzle axis and to expand at an angle 2θ.

The symmetry of the jet about the nozzle axis and its expansion at a constant jet angle are not universally accepted. This skepticism is justified by our experimental observations. Depending on the configuration of the pulsating jet, the half-angle (obtained from pictures of the transparent front plate of the apparatus) varied by as much as 4°.

Because the employment of the concept of a half-angle may simplify considerably the development of a flow model, an average jet half-angle was obtained for the three different series of tracer injection experiments. These values were compared with the constant value of $\theta \simeq 9.5°$ obtained from the analysis by Anagbo (1980) on the derivation of a jet cone angle from bubble theory (Table 4).

The value of the jet half-angle as a function of the kinematic

TABLE 4. JET HALF-ANGLE: EXPERIMENTAL VALUES AND COMPARISON WITH PREDICTIONS OF CORRELATIONS

Series No.	Experimental Jet Half-Angle (Figure 11)	Jet Half-Angle Eq. 8 (Rushton 1980; Donald & Singer, 1959)		Jet Half-Angle Eq. 9 (Merry, 1975)	
		θ^a	θ^b	θ^a	θ^b
1	8.7° ± 3.3°	10.4°	7.5°	14.9°	7.1°
2	7.9° ± 3.7°	10.4°	7.6°	14.9°	7.5°
3	7.3° ± 2.4°	10.4°	8.0°	14.9°	8.3°

[a] Effect of solids loading in injected stream not included.
[b] Effect of solids loading in injected stream included.

viscosity of the injected jet stream was calculated according to the correlation reported by Rushton (1980) and Donald and Singer (1959). Accordingly, the jet half-angle is given by:

$$\tan(\theta) = 0.238\nu^{0.135}, \tag{8a}$$

where ν, the kinematic viscosity of the jet stream in Stokes at the injection point, was calculated from the relation:

$$\nu = \frac{\mu_f \exp(5(1-\epsilon)/3\epsilon)}{\rho_{sf}(1-\epsilon) + \rho_f \epsilon}, \tag{8b}$$

using the results by Barnea and Mizrahi (1973) (Table 4). The jet half-angles predicted by the above correlation were also checked by comparing them with the measurements of jet cone angle ($2\theta \simeq 19$–$22°$) by Themelis et al. (1969) for air jets in water ($\nu_{air} \simeq 0.15 \rightarrow \theta \simeq 10.4°$).

The value of the jet half-angle was also calculated from the correlation developed by Merry (1975) as a function of the fluidized bed properties. Then, for the range $1 < \cot(\theta) < 13$,

$$\cot(\theta) = 10.4\left(\frac{\rho_s d_p}{\rho_f d_o}\right)^{-0.3}. \tag{9}$$

When the effect of solids loading in the injected fluid stream is taken into consideration, the value of ρ_f in Eq. 9 must be replaced by ρ_m (Eq. 7a). Comparison of the calculated values with our experimental results (see Table 4) confirms our visual observations of the narrowing of the jet half-angle when the injection of the tracer particles is initiated.

Jet Constriction Frequency

As stated earlier, for our flow conditions the jet was in a pulsating bubbling mode. In this mode the jet consisted of a series of coalescing bubbles with periodic constriction points at the points of coalescence. The bed material appeared to become entrained into the jet primarily through these constrictions, which moved upward and, in the process, were replaced by newly formed constrictions in the lower portion of the jet. High-speed movies of the lower jetting portion of the bed (up to 22 cm above the jet injection tube) showed that, for the flow conditions prevailing in the three series of tracer particle injection experiments, the first constriction point, which formed a few tube diameters downstream of the jet injection tube, moved upward with a constant speed of about 150 cm/s.

The frequency with which the first constriction point formed (f_{jc}) was obtained from high-speed movies (1,000 frames per second) of the lower portion of the jet for a range of jet injection flow rates while the flows through the grid and the annulus were maintained constant at 5.54×10^{-3} and 3.04×10^{-3} m^3/s, respectively. Our data indicated that the constriction formation frequency increased with increasing jet flow rate. (The jet flow rate was varied between 2.5×10^{-3} and 22.0×10^{-3} m^3/s.) The observed frequencies were of the order of 10 Hz, ranging from 5 Hz at the lowest jet flow rates to 20 Hz at the highest jet flow rates (Figure 13). The above observations are important for formulating a realistic model of the solid circulation induced by the presence of the jet, and they are in agreement with our conclusions on improved solids mixing with increased jet injection velocity.

Maximum Slugging Bed Height

The maximum bed height (H_{max}) during slugging may be theoretically predicted if we assume that the time taken for a bed to expand to the maximum height is equal to the time the slug takes to travel to the surface. The expression of Matsen et al. (1969) for the maximum slugging bed height can then be modified to include the presence of the jet by replacing the maximum and minimum bed heights by the difference between these heights and the height at which the slug forms (H_{SF}). Moreover, to take into consideration the fact that our column is semicircular and not circular, the tube diameter in the expression for bubble velocity U_b was replaced by the hydraulic diameter of the column D_h. Then,

$$\frac{H_{max} - H_{SF}}{H_{min} - H_{SF}} = 1 + \frac{U - U_{mf}}{0.35\sqrt{\beta g D_h}}, \tag{10}$$

$\beta = 1$ .... ideal slug (slug travels upward in the middle of the column) (Dumitrescu, 1943; Davies and Taylor, 1950)

$\beta = 2$ .... wall slug (slug travels upward attached, on one side, to the column wall) (Birkhoff and Carter, 1957; Stewart and Davidson, 1967).

$\beta = 0.04$ .. wall-to-wall slug (Stewart and Davidson, 1967; Matsen and Tarmy, 1970).

For design purposes, H_{SF} could be approximated by the jet penetration length.

Analysis of movies of the transparent cold flow model at 64 frames per second showed that during our experiments the slugs were predominantly initiated as stationary horizontal voids above the jet. These stationary horizontal voids increased in size with time before their transformation to wall slugs (Baeyens and Geldart, 1974) that subsequently moved through the bed and disappeared.

Our experimental observations for maximum slugging bed height compare favorably with the correlation of Eq. 10. The difference between the theoretically calculated values and the experimental observations is about 10% (Table 5).

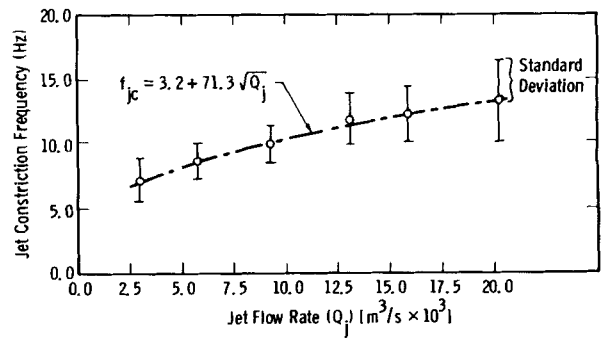

Figure 13. Jet constriction frequency as a function of jet flow rate (annular flow = 3.04×10^{-3} m^3/s; grid flow = 5.54×10^{-3} m^3/s).

TABLE 5. MAXIMUM SLUGGING BED HEIGHT

Series No.	$\frac{H_{max} - H_{SF}}{H_{min} - H_{SF}}$ Exp	$\frac{H_{max} - H_{SF}}{H_{min} - H_{SF}}$ Eq. 10: $\beta = 1$	$\frac{H_{max} - H_{SF}}{H_{min} - H_{SF}}$ Eq. 10: $\beta = 2$
1	1.4 ± 0.3	1.5 Error: 7%	1.3 Error: 7%
2	1.5 ± 0.3	1.7 Error: 13%	1.5 Error: 0%
3	1.9 ± 0.4	1.9 Error: 0%	1.7 Error: 11%

Slug Length and Frequency

The slugging mechanism plays an important role in the mixing of solids, especially in the slugging upper layers of our fluidized-bed reactor. The solids carrying capacity of the wake of the slug and its frequency of formation and detachment, together with the associated bulk solids movement, are the controlling phenomena in characterizing the solids circulation induced by slugging.

To obtain information about the slugging behavior of the reactor, experiments were conducted during which the airflows through the grid and annulus were maintained constant at 5.54×10^{-3} and 3.04×10^{-3} m^3/s, respectively, and the airflow through the jet was varied. Regular movies of the transparent cold flow model at 64 frames per second were taken and subsequently analyzed to provide information on slug length and slugging frequencies.

Slug Length. In an effort to relate the observed slug lengths to the flow conditions in the cold flow model reactor, existing correlations were modified to take into account three factors: a) the observed slugs were predominantly wall slugs; b) our test apparatus has a semicircular cross sectional area and, therefore, the hydraulic diameter D_h of the column is the pertinent length scale for slugging; and c) in most of the experiments reported here only a single slug was moving inside the column at a given time, the simultaneous presence of two moving slugs being a rare occurrence. Therefore, the height of the solids above the slug prior to its detachment, $h_s = TD_h$, is the quantity that determines the volume of the solids affected by the slug motion.

The analysis that led to the correlation for slug length as a function of reactor flow conditions is similar to the analyses of Nicklin et al. (1962) and Kehoe and Davidson (1970).

Assuming that the downward velocity of the emulsion phase with respect to the nose of the slug is given by $U_e = k_s\sqrt{2gy}$ at a distance y from the nose of the slug ($k_s = 1$ for an axisymmetric slug), and by writing a mass balance with respect to a coordinate system that moves with the surface of the slugging bed, we obtained the shape factor:

$$m = \frac{V_{sl}}{AD_h} = \frac{L_{sl}}{D_h} - \frac{0.495}{k_s}\sqrt{\frac{\beta L_{sl}}{D_h}} + 0.061, \qquad (11)$$

where β is defined in Eq. 10. Combining Eqs. 10 and 11 and noting that the increase in bed height from H_{min} to H_{max} is caused by the slug volume, i.e., $V_{sl}/V_e = (H_{max} - H_{min})/(H_{min} - H_{SF})$, we obtain the following equation for slug length in terms of the excess gas velocity $(U - U_{mf})$ and the nondimensional solids height T:

$$\frac{L_{sl}}{D_h} - \frac{0.495}{k_s}\sqrt{\frac{\beta L_{sl}}{D_h}} + 0.061 - T\left(\frac{U - U_{mf}}{U_b}\right) = 0. \qquad (12)$$

The nondimensional solids height was experimentally determined to be independent of the excess gas velocity. The value of T ranged between 2.6 and 4.0, with a time-averaged value of about 3.3. This is qualitatively in agreement with the findings of Baeyens and Geldart (1974), who found that when there is negligible bubble coalescence the interslug spacing was only a function of the bed diameter. On the other hand, if we assume T to be equal to the tangent of an aerated angle of internal friction of the solids, then, $T = \tan(73) = 3.3$, which is also in good agreement with our observations.

The observed nondimensional slug lengths (L_{sl}/D_h) are plotted in Figure 14 as a function of $(U - U_{mf})/0.35\sqrt{2gD_h}$. The best

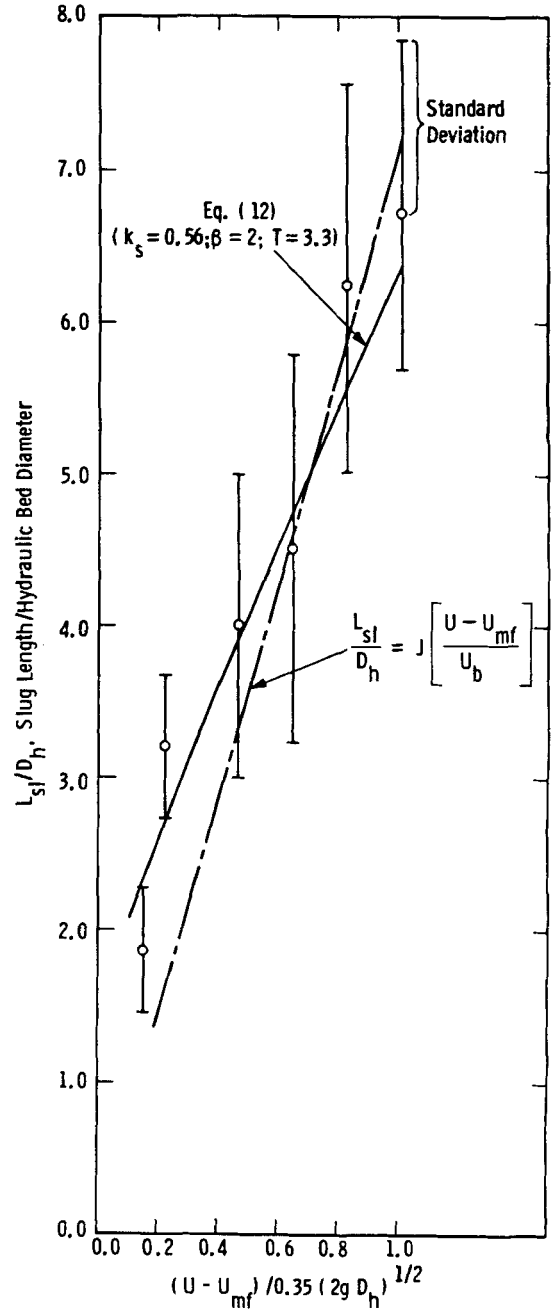

Figure 14. Slug length as a function of the excess gas velocity (variation in jet injection velocity).

fit between the data and the predictions of Eq. 12 was obtained for $k_s = 0.560$, which suggests a flatter average velocity profile in the emulsion phase with wall slugs than the one observed with axisymmetric or ideal slugs. The experimental results shown in Figure 14 support the observations of Thiel and Potter (1977), according to whom the criterion of Stewart and Davidson (1967) for the onset of slug flow [i.e., $(U - U_{mf})/U_b \geq 0.2$] must be applied with some care. For high aspect ratio beds, the reactor will certainly operate in the slug flow mode if the criterion is satisfied. If $(U - U_{mf})/U_b < 0.2$, however, it does not necessarily follow that the fluidized bed will be freely bubbling.

Slug Frequency. For the experimental range of values of $(U - U_{mf})/U_b$, L_{sl}/D_h can be expressed by the approximation:

$$\frac{L_{sl}}{D_h} = J\frac{U - U_{mf}}{U_b}, \qquad (13)$$

where the value of J was obtained from our experimental observations to be 7.163. Then, the corresponding slug frequency, i.e.,

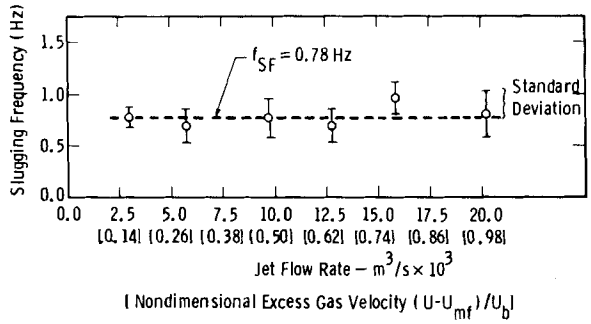

Figure 15. Slugging frequency as a function of jet flow rate (annular flow = 3.04×10^{-3} m³/s; grid flow = 5.54×10^{-3} m³/s) and corresponding nondimensional excess gas velocity.

the number of slugs passing a given axial position per unit time, is given by:

$$f_{SF} = \frac{0.35}{J}\sqrt{\frac{\beta g}{D_h}}. \tag{14}$$

The expression of Eq. 14 shows that the slugging frequency is independent of the gas superficial velocity. For $J = 7.163$, f_{SF} is calculated to be 0.52 Hz. As shown in Figure 15, the observed slug frequencies are insensitive to variations in the jet flow rate. The value of f_{SF} calculated from Eq. 14 is in satisfactory agreement with the experimental value of f_{SF} = 0.78 Hz.

Experiments conducted to obtain slug frequencies as a function of the grid and annular flows yielded very similar results with f_{SF} = 0.71 Hz and f_{SF} = 0.65 Hz, respectively.

Mixing Time

Knowledge of the time required for the solids to attain the well-mixed condition as a function of controlling flow field variables is essential for the prediction of reactor performance by properly modeling the fluidized-bed hydrodynamics as compared with the observed reaction kinetics.

During our experiments the time required for the injected solids to attain the well-mixed condition decreased with increasing gas superficial velocity. Realizing that slugging is probably the hydrodynamically limiting mechanism for solids mixing, we plotted the nondimensional mixing time $\tau/(1/f_{SF})$ versus the nondimensional excess gas velocity $(U - U_{mf})/U_b$ on a log-log plot. As shown in Figure 16, the three experimental points fall on a straight line and, therefore, our findings on solid mixing time can be correlated with the empirical expression:

$$\frac{\tau}{(1/f_{SF})} = 6.5\left(\frac{U - U_{mf}}{U_b}\right)^{-5/3}. \tag{15}$$

Data Reproducibility

The reproducibility of the results reported in this paper was assessed and the following conclusions were drawn:

a) The gross flow field characteristics obtained from studying the movies of the cold flow unit (this includes jet penetration length, slug length, slug frequency, jet half-angle) were reproducible within the degree of error (due to the oscillating nature of the gas-particle dynamics) shown in the respective figures or tables.

b) The jet penetration length obtained after defluidization from the maximum in the tracer concentration profile of a short duration tracer injection was reproducible for each run within the error incurred due to the oscillatory nature of the jet (see Table 3).

c) For a given jet injection velocity, the weight of tracers that arrived at either the top of the jet (maximum in tracer concentration profile) or the top layers of the bed that had uniform radial concentration profiles (slug region) was proportional to the injection time, with the factor of proportionality being different for each jet injection velocity. The effect of the periodic nature of the gas-particle dynamics on the tracer concentration was not appreciable compared to the observed time-averaged trend. As expected, the effect of the oscillatory nature of the gas-particle dynamics was more pronounced at the lowest jet injection velocity and for the shortest tracer particle injection duration, the reproducibility of the data being the best at the highest jet injection velocity of 52 m/s and for the longest tracer particle injection duration.

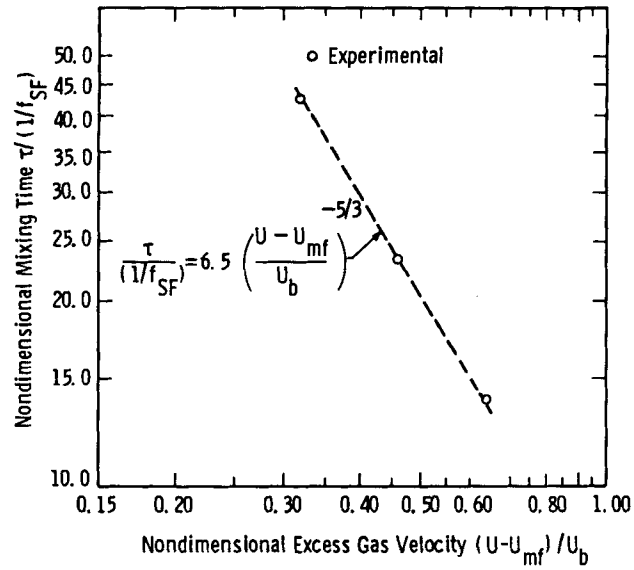

Figure 16. Nondimensional mixing time as a function of nondimensional excess gas velocity.

ACKNOWLEDGMENT

The support provided by DOE Contract DE-AC01-80ET10161 is gratefully acknowledged. We also wish to express our appreciation to A. W. Fellers for his assistance in setting up and conducting the experiments and to J. McKenzie for his assistance in taking the movies.

NOTATION

A = cross-sectional area of apparatus

$\overline{C}_T$ = $[W_T/(W_B + W_T)]/[W_T/(W_B + W_T)]_{\text{total}}$ = Weight fraction of tracer particles in sampled volume/Weight fraction of tracer particles in entire bed

D_b = diameter of bubble generated at the end of the jet

D_h = hydraulic bed diameter; $D_h \equiv \dfrac{4A}{\frac{1}{2}\pi D_t + D_t} = 0.611\, D_t$

D_t = diameter of semicircular experimental apparatus

d_o = jet injection tube diameter

d_p = mean particle diameter of bed solids

d_{RMS} = root-mean-square deviation from well-mixed condition (Eq. 1)

f_{jc} = frequency of formation of first jet constriction downstream of the jet injection tube

f_{SF} = slugging frequency (Hz)

g = acceleration of gravity

$H_{\max}$ = maximum slugging bed height (time-averaged value)

H_{mf} = bed height at minimum fluidization condition when no central jet is present

$H_{\min}$ = minimum slugging bed height (time-averaged value)

H_{SF} = height at which the slug forms and detaches from the jet

h_s = height of granular bed solids above the slug prior to slug detachment and motion

J = empirical coefficient relating slug length to excess gas velocity (Eq. 13)

k_s = empirical emulsion phase velocity shape factor in the slug region; $U_e = k_s\sqrt{2gy}$

L = height of solids stagnation zone around jet measured from jet injection tube (see Figure 10)

L_j = jet penetration length (time-averaged value)

$L_{\max}$ = maximum observed jet penetration length for given flow conditions

$L_{\min}$ = minimum observed jet penetration length for given flow conditions

L_{MC} = average defluidized-bed height at which the tracer concentration is maximum for short tracer injection durations

L_{sl} = slug length

M_f = mass flux of injected gas

M_{sj} = mass flux of injected solids

Q_j = gas flow rate through jet injection tube

T = nondimensional height of granular bed solids above the slug prior to slug detachment and motion; $(T = h_s/D_h)$

U = superficial gas velocity

U_b = bubble rise velocity = $0.35\sqrt{\beta g D_h}$

U_{cf} = superficial gas velocity at complete fluidization conditions

U_e = downward velocity of emulsion phase with respect to the nose of the slug; $U_e = k_s\sqrt{2gy}$

U_f = velocity of injected gas at jet injection point

U_m = gas-solid mixture velocity at jet injection point [Eq. (7b)]

U_{mf} = superficial gas velocity at minimum fluidization conditions

U_{sj} = velocity of injected solids at jet injection point obtained by analyzing the high-speed movies taken at 1,000 frames per second

U_t = terminal particle velocity

V = volume of sampled bed solids

V_e = volume of the emulsion phase in the slugging portion of the bed

V_j (V_{jet}) = volume occupied by the jet (Figure 12)

V_s = volume of solids in the emulsion phase around the jet (Figure 12)

V_{sl} = slug volume

W_B = weight of bed material in sampled layer

W_T = weight of tracer material in sampled layer

$W_{B_{\text{total}}}$ = total weight of bed material present inside the cold-flow model

$W_{T_{\text{total}}}$ = total weight of tracer material injected into the cold-flow model during a tracer injection experiment

x_i = weight fraction of particle-size fraction i

Greek Letters

α = angle of cone of influence of jet (Figure 10); internal angle of friction (Zenz, 1960)

β = constant defined in Eq. 10

ϵ = void fraction at jet injection point

ϵ_B = average void fraction in emulsion phase around jet (Figure 12)

ϵ_{jet} = average void fraction in jet (Figure 12)

ϵ_{mf} = void fraction at minimum fluidization

θ = jet half-angle (time-averaged value)(Figure 10)

μ_f = gas viscosity

ν = kinematic viscosity of the injected jet stream in Stokes (cm^2/s) (Eq. 8b)

ρ_f = gas density

ρ_m = gas-solid mixture density at jet injection point (Eq. 7a)

ρ_s = density of solid particles in bed

ρ_{sj} = density of injected solid particles

τ = time needed for the pneumatically injected solids to attain well-mixed condition

LITERATURE CITED

Anagbo, P. E., "Derivation of Jet Cone Angle from Bubble Theory," *Chem. Eng. Sci.*, **35**, 1494 (1980).

Baeyens, J., and D. Geldart," An Investigation into Slugging Fluidized Beds," *Chem. Eng. Sci.*, **29**, 255 (1974).

Barnea, E., and J. Mizrahi, "A Generalized Approach to the Fluid Dynamics of Particulate Systems. Part 1: General Correlation for Fluidization and Sedimentation in Solid Multiparticle Systems," *Chem. Eng. J.*, **5**, 171 (1973).

Birkhoff, G., and D. Carter, "Rising Plane Bubbles," *J. Rat. Mech. Anal.*, **6**, 769 (1957).

Davidson, J. F., and D. Harrison, *Fluidised Particles*, Cambridge University Press, London, 1963, p. 50–62.

Davies, R. M., and G. I. Taylor, "The Mechanics of Large Bubbles Rising through Extended Liquid and through Liquids in Tubes," *Proc. Roy. Soc., London*, **A200**, 375 (1950).

Donald, M. B., and H. Singer, "Entrainment in Turbulent Fluid Jets," *Trans. Inst. Chem. Engrs.*, **37**, 255 (1959).

Dumitrescu, D. T., "Stromung an einer Luft-blase im senkrechten Rohr," *Z. Angew. Math. Mech.*, **23**, 139 (1943).

Geldart, D., "Types of Gas Fluidization," *Powder Tech.*, **7**, 285 (1973).

Hirsan, I., C. Sishtla, and T. M. Knowlton, "The Effect of Bed and Jet Parameters on Vertical Jet Penetration Length in Gas Fluidized Beds," 73rd Annual AIChE Meeting, Chicago (Nov. 16–20, 1980).

Hogg, R., and D. A. Augenstein, "Rheology of Free Flowing Powders," Proceedings, 1978 Powder and Bulk Solids Conference, Rosemont, IL (May, 1978).

Kehoe, P. W. K., and J. F. Davidson, "Continuously Slugging Fluidized Beds," 'Chemeca 70', Chemical Engineering Conference, Australia, Butterworth & Co., (Australia) Ltd., Sec. 1, p. 97 (1970).

Knowlton, T. M., and I. Hirsan, "The Effect of Pressure on Jet Penetration in Semi-Cylindrical Gas-Fluidized Beds," *Fluidization*, Proc. of the 3rd Engineering Foundation Conference, 315, Plenum Press, New York (1980).

Matsen, J. M., S. Hovmand, and J. F. Davidson, "Expansion of Fluidized Beds in Slug Flow," *Chem. Eng. Sci.*, **24**, 1743 (1969).

Matsen, J. M., and B. L. Tarmy, "Scale-up of Laboratory Fluid-Bed Data: The Significance of Slug Flow," *Chem. Eng. Prog. Symp. Ser.*, No. 101, **66**, 1 (1970).

Merry, J. M. D., "Penetration of Vertical Jets into Fluidized Beds," *AIChE J.*, **21**(3), 507 (1975).

Nicklin, D. J., J. D. Wilkes, and J. F. Davidson, "Two-Phase Flow in Vertical Tubes," *Trans. Inst. Chem. Eng.*, **40**, 61 (1962).

Rowe, P. N., A. W. Nienow, and A. J. Agbim, "Mechanisms by which particles segregate in gas-fluidized beds. Binary systems of near-spherical particles," *Trans. Inst. Chem. Eng.*, **50**, 310 (1972).

Rushton, J. H., "The Axial Velocity of a Submerged Axially Symmetrical Fluid Jet," *AIChE J.*, **26**(6), 1038 (1980).

Stewart, P. S. B., and J. F. Davidson, "Slug Flow in Fluidized Beds," *Powder Tech.*, **1**, 61 (1967).

Themelis, N. J., P. Tarassof, and J. Szekely, "Gas-Liquid Momentum Transfer in a Copper Converter," *TMS-AIME*, **245**, 2425 (1969).

Thiel, W. J., and O. E. Potter, "Slugging in Fluidized Beds," *Ind. Eng. Chem., Fund.*, **16**(2), 242 (1977).

Wen, C. Y., N. R. Deole, and L. H. Chen, "A Study of Jets in a Three-Dimensional Gas Fluidized Bed," *Powder Tech.*, **31**(2), 175 (1982).

Yang, W.-C., and D. L. Keairns, "Design and Operating Parameters for a Fluidized Bed Agglomerating Combustor/Gasifier," 208, *Fluidization*, Eds., J. F. Davidson and D. L. Keairns, Cambridge University Press, Cambridge (1978).

Yang, W.-C., "Jet Penetration in a Pressurized Fluidized Bed," *Ind. Eng. Chem., Fund.*, **20**(3), 297 (1981).

Zenz, F. A., and D. F. Othmer, *Fluidization and Fluid Particle Systems*, Ch. #2, Reinhold Publishers, New York (1960).

Manuscript received January 4, 1982; revision received January 31, 1983, and accepted February 9, 1983.